2024 IEEE/RSJ International Conference on Intelligent Robots and Systems (IROS)
October 14-18, 2024. Abu Dhabi, UAE

Realistic Rainy Weather Simulation for LiDARs in CARLA Simulator

Donglin Yang*, Xinyu Cai*†, Zhenfeng Liu, Wentao Jiang, Bo Zhang,
Guohang Yan, Xing Gao, Si Liu†, Botian Shi

***Abstract*— Data augmentation methods to enhance perception performance in adverse weather have recently attracted considerable attention. Most of the LiDAR data augmentation methods post-process the existing dataset by physics-based models or machine-learning methods. However, due to the limited environmental annotations and the fixed vehicle trajectories in existing datasets, it is challenging to edit the scene and expand the diversity of traffic flow and scenario. To this end, we propose a simulator-based physical modeling approach to augment LiDAR data in rainy weather, enhancing the performance of the perception model. We complete the modeling task of the rainy weather effect in the CARLA simulator and establish a data collection pipeline for LiDAR. Furthermore, we pay special attention to the spray generated by vehicles in rainy weather and simulate this phenomenon through the Spray Emitter method we developed. In addition, considering the influence of different weather conditions on point cloud intensity, we develop a prediction network to forecast the intensity of the LiDAR echo. This enables us to complete the rainy weather simulation of 4D point cloud data. In the experiment, we observe that the model augmented by our synthetic dataset improves the performance for 3D object detection in rainy weather. Both code and dataset are available at https://github.com/PJLab-ADG/PCSim#rainypcsim.**

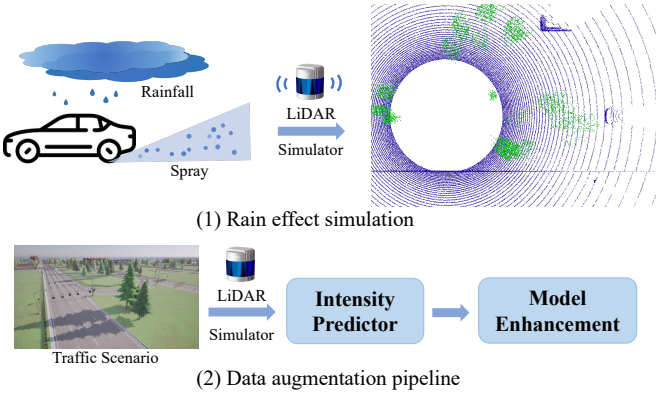

Fig. 1: In our simulation environment, we model the effects of rainfall and spray phenomena using a simulator-based physical modeling approach. We establish a data generation pipeline for rainy highway scenarios, where we add point cloud intensity using the Intensity Predictor. This process significantly contributes to synthetic data augmentation for 3D object detection tasks in rainy weather conditions.

I. Introduction

In adverse weather conditions, the perception performance of sensors in autonomous driving vehicles generally deteriorates. Limited by LiDAR's working principle, the effective detection distance of LiDAR decreases and the noise increases under fog, rain, snow, and other weather conditions [1], [2], [3]. Especially, in the case of water, snow, etc. on the road, the LiDAR detection system may detect a large number of droplets or snow particles sprayed or splashed from the back and side of vehicles, causing the LiDAR perception model to judge it as phantom obstacles, reducing the detection precision. Therefore, it is essential to make up for the defects in the point cloud data under adverse weather conditions through the autonomous driving perception algorithm and enhance the robustness of the perception algorithm.

With the increasing demand for datasets in terms of both quantity and quality, data augmentation methods of adverse weather are continuously emerging [4], [5], primarily involving techniques such as effect into existing datasets or generation from simulated environments. Some previous research has explored simulation methods for camera data, collecting RGB data under adverse weather conditions through simulation or generation, to minimize domain gaps as much as possible [6], [7], [8]. Recently, there have also been studies augmenting adverse weather conditions for point cloud data, proposing methods to simulate LiDARs in rain [9], [10], [11], fog [12], [13] and snow [14]. However, these methods cannot arbitrarily generate weather-affected data, as most rely on post-processing algorithms based on physical principles and use real point cloud data captured in clear weather conditions as input. Additionally, they are unable to replicate dynamic phenomena associated with specific weather conditions, such as spray phenomena in rain.

To address these challenges, this paper presents a simulation method for LiDAR data under rain conditions, as shown in Figure 1. We model the dynamic scene of rainy weather in the CARLA simulator [15] and directly generate large-scale point clouds with rainy weather noise. Specifically, we simulate the spray phenomenon occurring behind vehicles traveling at high speeds. However, due to the simulator's inability to accurately calculate LiDAR echo intensity, we propose a weather-based point cloud intensity prediction network to generate 4D point cloud data. This network

* Equal Contribution.
† Corresponding Authors.
This work was performed when the first author was interning at Shanghai Artificial Intelligence Laboratory.
Donglin Yang, Wentao Jiang, and Si Liu are with Beihang University. {yangdonglin, jiangwentao, liusi}@buaa.edu.cn
Donglin Yang, Xinyu Cai, Bo Zhang, Guohang Yan, Xing Gao and Botian Shi are with Shanghai Artificial Intelligence Laboratory. {yangdonglin, caixinyu, zhangbo, yanguohang, gaoxing, shibotian}@pjlab.org.cn
Zhenfeng Liu is with Nankai University. 2120220408@mail.nankai.edu.cn

predicts the intensity based on multi-channel input, including RGB images, semantic labels, point cloud data, and weather information.

We have developed a comprehensive data generation pipeline to achieve a high level of consistency between synthetic and real datasets, particularly for point cloud data augmentation under adverse weather conditions. Furthermore, we support real-time simulation, ensuring efficiency in generating simulated data and we can achieve more realistic sensor data through parameter configurations.

Our contributions are summarized as follows:

- We complete the modeling task of a rainy weather scene in the CARLA simulator, In particular, we pay attention to the spray caused by the wheels of surrounding vehicles and simulate this phenomenon through our Spray Emitter.
- We study the influence of weather conditions on the point cloud intensity, and establish an intensity prediction network to complete the 4D LiDAR point cloud simulation.
- We develop a LiDAR data generation pipeline under rainy weather and introduce a synthetic point cloud dataset, encompassing data from various rainfall highway scenarios. We utilize the dataset for data augmentation in the 3D object detection task and observe that it significantly improves the 3D object detection model's robustness to rainy conditions.

II. Related Work

A. LiDAR Simulation in Adverse Weather

LiDAR simulation in adverse weather aims to generate extra large-scale point cloud data that is challenging to collect and annotate in the real world to enhance models from a data-driven perspective. To achieve this, work has been done to simulate LiDAR data under rainy, snowy, and foggy weather [10], [11], [12], [14], [16]. to make the perception models more robust in varying weather conditions, despite shortcomings in the original training dataset. Yang *et al.* [16] published a method to simulate foggy conditions within the collected LiDAR data. Moreover, Hahner *et al.* [12], [14] developed physically based models in the power signal domain for fog and snowy conditions and improved 3D object detection performance through data augmentation to expand the dataset. Goodin *et al.* [10] present a simplified model to simulate the LiDAR performance in rain, while Kilic *et al.* [11] present a comprehensive approach for adverse weather conditions based on Mie theory [17].

In contrast to previous post-processing methods that augment existing datasets from clear conditions, our approach employs a simplified model and establishes a dedicated pipeline for the direct acquisition of synthetic point cloud data. Leveraging the simulator's advantages, we can reproduce dynamic weather phenomena and obtain precise labeling information.

B. Spray Effect Simulation

Spray simulation is receiving increasing attention in pursuing autonomous driving due to the substantial noise it introduces to LiDAR data. Rivero *et al.* [18] presents a real-time simulation of the spatial distribution of detection on spray effect. Other approaches utilize physical models of spray to conduct simulations. The early research was established by Weir [19], which categorized the generation of spray phenomenon into four mechanisms. Shih *et al.* [20] reconstructs spray patterns and synthesizes spray data by trajectory simulation and matching algorithms. Linnhoff *et al.* [21] proposed a clustering method for spray generation, and analyzed the disturbance pattern from real data. They also evaluate the improvement of LiDAR-based detectors trained with artificial spray data. Compared to the previous work, we utilize a physical model to simulate spray within the simulator in real-time.

C. Point Cloud Intensity

The point cloud intensity captured by LiDAR constitutes a vital aspect of 3D detection and segmentation. LiDAR intensity is influenced by the geometric, physical, and environmental attributes of the LiDAR system. Dropout noise, resulting from light absorption and scattering, significantly impacts the quality of LiDAR data, with notable consequences for 3D perception. Wu *et al.* [22] proposed a point cloud intensity simulation method to obtain a dataset from a game engine. In a related development, Manivasagam *et al.* [23] employed U-net architecture to output a ray drop probability, and framed the LiDAR ray drop problem as a binary classification task. Vacek *et al.* [24] proposed a method to model intensity using a combination of LiDAR geometry, RGB images, and semantic labels. Compared with the previous works, our focus is on the study of intensity prediction under varying rainy weather conditions.

III. Physics Based Point Cloud Simulation in Rainy Weather

In the field of autonomous driving, LiDAR systems are often affected by two types of droplets generated by rainfall: one is global, raindrops falling from clouds distributed throughout the entire environment, the other is localized, resulting from interactions between other moving objects and the environment. After encountering rain droplets, LiDAR typically experiences false echoes and signal attenuation, resulting in increased noise and decreased perception range.

For the global droplet effects, there have been prediction and augmentation methods [10], [11], developing physics models to calculate the effect of droplets on LiDAR echoes. We integrated Kilic's hybrid Monte Carlo approach [11] into the LiDAR of the simulator to simulate the global effects of rainfall. Additionally, we adopted [14]'s wet ground model to simulate the phenomenon of loss points on wet road surfaces.

Regarding the simulation of localized droplet effects in rainy conditions, we have emphasized the spray phenomenon. This phenomenon generates a large quantity of raindrops, characterized by small raindrop diameters and

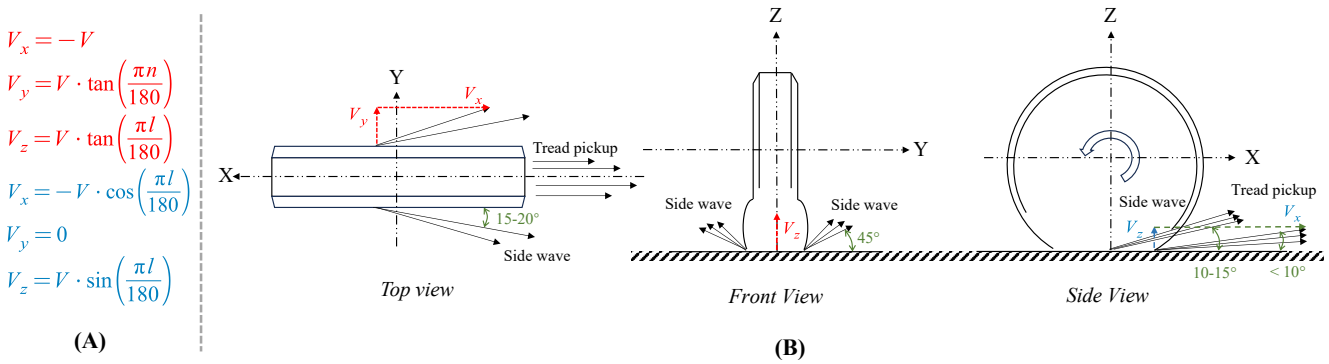

Fig. 2: **(A)** Calculation of velocity components projected onto Cartesian coordinates where n represents the angle between the velocity projected onto the XOY plane and the negative X-axis, while l represents the angle between the velocity projected onto the XOZ plane and the positive X-axis. **(B)** Spray Phenomenon Mechanism Analysis through top, front, and side views. The velocities of tread pickup and side wave are respectively in blue and red.

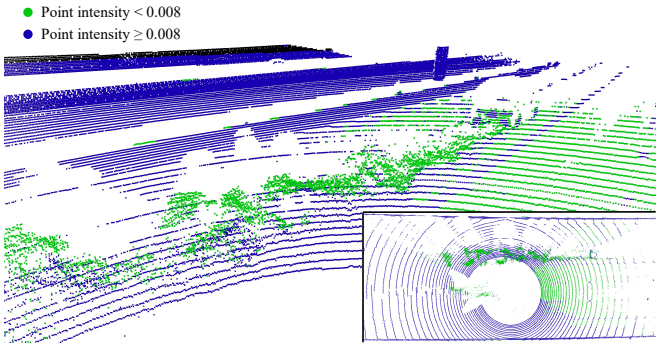

Fig. 3: Visualization with spray phenomenon from Waymo dataset [25] (points with intensity value below 0.008 in green, and other points in blue). While intensity-based filtering removes a substantial amount of the spray noise points, it also results in the filtering of points corresponding to vehicles and roads. The bottom right image depicts a point cloud view from the Bird's Eye View (BEV) perspective.

clustered distribution, with varying shapes susceptible to influences such as wind and turbulence. It can be seen in Figure 3 that these raindrops can introduce significant noise in LiDAR systems and may even obstruct vehicles or objects behind the spray, thereby impacting the performance of perception models and potentially leading to false detection [18]. Through an analysis of the point cloud data obtained from LiDAR-detected spray droplets in Waymo Open Dataset [25], we have estimated that the intensity of the spray points is typically less than 0.008. Despite its low intensity, mitigating the influence of this noise on perception models poses a challenge. Basic methods based on intensity filtering of the point cloud, as illustrated in Figure 3, may incorrectly filter out the point cloud data of objects behind the spray, resulting in the loss of valuable information.

Therefore, in the following subsections, we introduce a simulator-based physical modeling approach, the Spray Emitter to generate point cloud data with localized droplet noise of spray phenomenon.

A. Spray Amount Modeling

In the stagnant water scene caused by heavy rain, the mechanisms of spray water caused by flying tires can be divided into bow wave, capillary adhesion, tread pickup, and side wave [19]. Due to the obstruction of the vehicle chassis and tire muddy plates, the droplets caused by bow wave and capillary adhesion will quickly vanish due to collision. The tread pickup droplets are generated from the stagnant water attached to the tire gully. When the vehicle is running, the water in the tire drainage groove will rotate with the wheel at high speed, and finally spray out in the form of spray water on the rear side of the tire. Meanwhile, side wave may result in anomalies in vehicle point cloud contours. Therefore, we consider tread pickup and side wave as our primary areas of research, as shown in Figure 2. When LiDAR is operating, tread pickup droplets and side wave will form a barrier between the laser rays and the target, generating a large number of noise point clouds.

The amount of spray water is mainly related to the speed of the vehicle and the depth of the water film on the ground. The amount of tire gully water increases with the depth of the water film until reaching the depth of the gully. When the speed is increased, the jet frequency of tread pickup will become higher and higher, resulting in a more significant spray phenomenon. The water volume of each mechanism can be described as shown in Equation 1 and as introduced by Weir [19] *et al.*

$$\begin{aligned} VR_{TP} &= Kbvh_{groove} \\ VR_{SD} &= 0.5bv(WD - Kh_{groove} - (1-K)h_{film}) \\ WD &= 6e^{-4}T^{0.09}(LI)^{0.6}S^{-0.33} \end{aligned} \tag{1}$$

where VR_{TP} and VR_{SD} respectively denote the volume rate of each mechanism. K is the groove width proportion of the tire. h_{groove} is the depth of water in the tire tread, and h_{film} is the depth of water picked up on each rotation of the tire. WD is the water film thickness, calculated from an empirical formula [19], where T is the road texture depth, L is the drainage length, I represents rain rate and S represents the slope of road.

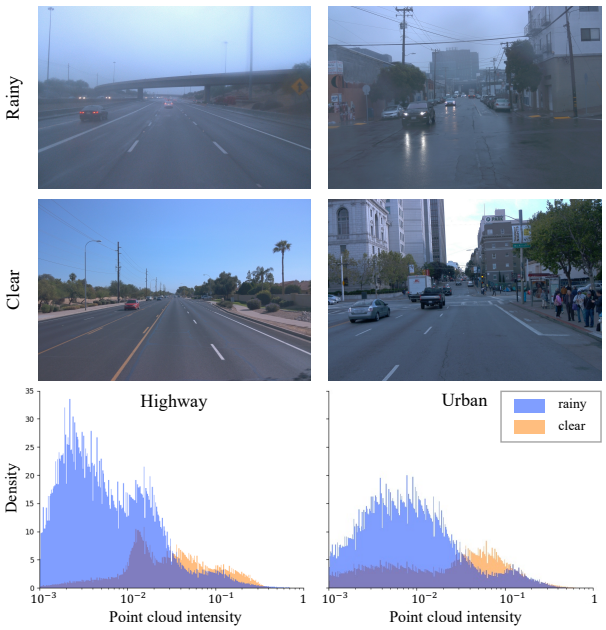

Fig. 4: Comparison of the point cloud intensity histograms under different weather conditions across highway and urban road scenes in Waymo dataset [25]. To minimize the impact of background objects, we select similar scenes with comparable traffic density and environmental features.

However, the uneven ground will lead to an increase in the randomness of the water depth. From Waymo Open Dataset [25], we can observe that the morphology of the spray changes in Figure 3, and the spray phenomenon exhibits a certain degree of randomness and unevenness. As a result, we add a time-varying weight to the water volume to simulate the randomness.

In the spray phenomenon, various droplet sizes can be observed. General statistical experiments [26], [27], [28], [29] show that most of the droplet sizes in spray water range from 0.2 mm to 6 mm. The average value is about 1 mm. To facilitate realistic simulation, we assume that the droplet is a perfect sphere of radius of 1 mm in our simulation method.

B. Spray Droplets Dynamic Model

When the droplets are out of the tires, they will be influenced by the wind, gravity, and turbulence at the rear of vehicles. Affected by the wake flow of a vehicle with high speed, spray or splash droplets swing along with the turbulence behind the vehicle. Yan *et al.* [30] analyzes the wake topology of the vehicle, which presents a bi-stable behavior. Airflow behind the vehicle is asymmetrical, while it is still statistically symmetrical over a long timescale. In response to this phenomenon, we adjust the mass flow rate of the two rear wheels, so that the spray phenomenon can present an instantaneous asymmetric spatial distribution. Meanwhile, to simulate the spray droplets' asymmetric trajectory, we introduced an initial lateral velocity for the droplets, whose direction is perpendicular to the vehicle's forward direction. Then we apply a horizontal constraint force to attenuate the lateral velocity. In addition to the turbulent force, the superposition of multiple forces such as the crosswind of the road, gravity, and air resistance, will continuously change the motion state of the spray water during the flight, forming an indeterminate particle group, to simulate its aerodynamic effect more realistically. During the flight process, the spray droplets disperse upon colliding with any object or surpassing a predetermined survival time. According to the emission quantities, the emission speed, and the force analysis above, we develop a physics-based model for spray phenomena. Ultimately, we employ ray projection LiDAR [15] to detect the reflection echoes of droplets and generate point cloud data.

IV. Weather-based LiDAR Intensity Predictor

In the point cloud data collected by LiDAR, The intensity is the strength of the return power received by the LiDAR detector. The return power P_r generally represents:

$$P_r = P_t \Omega \rho \eta_{sys} \eta_{atm} \tag{2}$$

P_t is the transmitted power. Ω is the scattering steradian solid angle of the target, which inversely scales with the square of the target distance. ρ is the reflectance of the target surface, while η_{sys} represents the efficiency values of the optics of system, and η_{atm} denotes atmospheric attenuation. Furthermore, as shown in Figure 4, weather conditions are the primary factor contributing to the differences in point cloud intensity distribution. In rainy weather, the point cloud intensity distribution shifts towards lower values. Specifically, in highway scenes under rain, the point clouds exhibit the highest density around 2×10^{-3} due to the influence of spray phenomena. Therefore, we present a weather condition-based intensity predictor by integrating the factors in Equation (2).

A. Intensity Prediction Neural Network

Following the approach proposed by [22], [24], we utilize a U-net [31] neural network to learn point cloud intensity from real data. As illustrated in Figure 5, we take multi-modal data as input. We leverage the network's ability to implicitly learn object information from RGB images and semantic labels. Additionally, we input LiDAR depth and rain conditions to implicitly obtain the solid angle Ω and atmospheric attenuation η_{atm} to predict point cloud intensity.

All data input to the intensity predictor is represented in the LiDAR spherical coordinate system and organized in the form of a multi-channel range image. Same as [24], we project the sparse LiDAR point cloud onto the five camera images in the Waymo dataset [25] to obtain RGB information. We acquire the semantic labels from the Waymo dataset [25] and CARLA simulator. To facilitate training and inference on both the Waymo dataset [25] and synthetic dataset, we utilize the intersection of two semantic categories, including 12 categories such as 'unlabeled', car, bicycle, pedestrian, road, building, and vegetation. For each sequence in the Waymo dataset [25], we annotated four levels of rain conditions including clear, wet ground, light rain, and heavy rain.

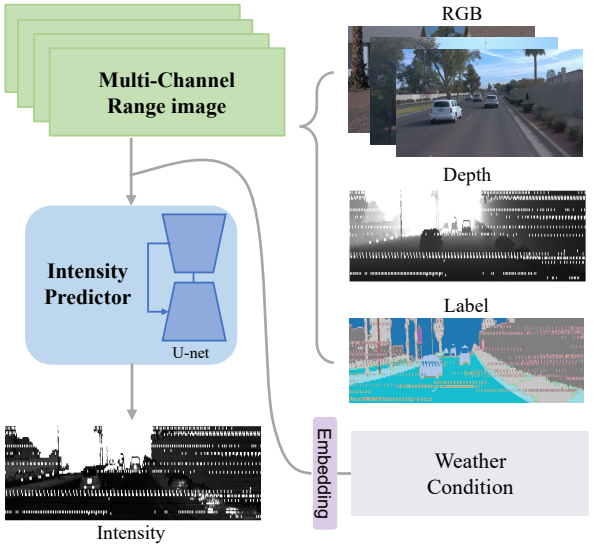

Fig. 5: Intensity Predictor Pipeline. Following the projection and embedding processing, the input of the predictor is organized as a multi-channel range image. We apply the encoder and decoder structures of U-net to predict point cloud intensity.

We introduce the RGB mask and drop-off mask to denote the absence of RGB values or missing points in the point cloud and supervise the intensity predictor using masked L2 loss.

$$\mathscr{L}_2 = \mathbf{MSE}(\hat{I},\ I) \cdot M \tag{3}$$

where $\hat{I}$, I denote the predicted intensity range image and ground truth intensity range image, and M is the union of RGB mask and drop-off mask.

B. Model Validation

Input Channel	Image Size	Intensity MSE ↓		
		Overall	Light Rain	Heavy Rain
RGB+D+L	64×640	0.0075	0.0051	**0.0046**
RGB+D+L+W	64×640	**0.0071**	**0.0051**	0.0049
RGB+D+L	64×1376	0.0089	0.0068	0.0060
RGB+D+L+W	64×1376	**0.0082**	**0.0052**	**0.0059**

TABLE I: Additional weather input analysis using intensity MSE, where Overall denotes the result across all weather conditions, including sunny, light rain, and heavy rain.

We compared the predicted intensity with the ground truth intensity in Waymo dataset [25] by using the mean squared error (MSE) metric, the result is shown in Table I. All experiments shared the same setup, including an initial learning rate of 0.01, the utilization of a cosine decay learning strategy, and a weight decay value set at 0.01. We evaluate the impact of the input of weather conditions and different widths of range images on the intensity predictor. Adding weather conditions reduces the predictor's errors, with errors decreasing as precipitation intensity increases. Similarly, we conducted experiments using a wider field of view spanning about 180 degrees, *i.e.*, range image size of 640×1376, and observed that the input channel of the rainy condition has a more pronounced effect on the model.

V. Experiments

A. Point Cloud synthetic dataset in Adverse Weather

We leverage the realistic autonomous driving simulator CARLA [15] to implement the above approach. Specifically, we employ the blueprint visual scripting system and a realistic LiDAR model to generate the simulated rain effect. We add a Spray Emitter component to the base vehicle blueprint in the simulator. The Spray Emitter utilizes the information acquired from the simulator including the position of the vehicle's rear wheels, vehicle speed, map data, and weather parameters, to generate and control the spray droplets, achieving high-quality, dynamic simulation of the spray phenomenon.

To narrow the domain gaps between the synthetic point cloud data and real-world data, we extend Waymo LiDAR to the RLS library [32] and complete the LiDAR model with rain effect in the simulator. According to the information described by Waymo Open Dataset [25], we configured Waymo LiDAR as a mechanical rotating system, emitting around 1.6 million lasers per second, and achieving a maximum effective detection distance of 75 meters. Its vertical field of view spans from -17.6 to +2.4 degrees, and it is positioned at 2 meters in the vehicle coordinate system.

In selecting simulation scenarios, we opt for highway scenarios that are more susceptible to the effects of rainy weather. In urban roads, the impact of heavy rain on LiDAR is mainly from the droplets in the landing. However, on highway segments, the occurrence of spray becomes more widespread and intense due to the higher speed of vehicles, posing greater challenges to LiDAR systems. During the generation of the synthetic dataset with the CARLA simulator, we primarily selected the map named Town07 as our simulation environment, which features a higher density of highway segments. We control the traffic flow within the perception range of our ego vehicle and periodically generate a certain number of additional vehicles, ensuring the realism and effectiveness of the collected data. In this scene, the vehicle speed ranges from 80km/h to 100km/h, and the rainfall is from 30mm/h to 60mm/h.

We utilize OpenCDA, the data collection framework [33] to simultaneously collect LiDAR data, semantic LiDAR data, panoramic view of RGB images, and weather and vehicle labeling information. We collect a total of 10k frames of data as a synthetic rainy dataset under various rainfall conditions at 10 Hz. Specifically, we partition synthetic data into front and rear 180-degree views. We then use the predictor trained on Waymo dataset's [25] forward 180-degree data to make inferences on these segments, ultimately generating complete 4D point cloud data. We statistically analyze the point cloud intensity distribution shown in Figure 4. We consider that the intensity of spray noise follows a distribution around the peak of the point cloud intensity observed in rainy highway scenes, and employ a Gaussian distribution to fit this pattern.

Setting		Clear Weather Test Set				Rainy Weather Test Set			
		AP@.5IoU		AP@.7IoU		AP@.5IoU		AP@.7IoU	
Additional Data Source	Samples	BEV	3D	BEV	3D	BEV	3D	BEV	3D
Waymo Rainy Dataset	0 (baseline)	81.4	78.63	**74.81**	55.98	80.5	77.24	73.78	35.61
	2k	79.32	**78.93**	73.17	57.33	81.70	78.41	75.08	38.01
	4k	**81.52**	78.85	73.16	**57.9**	**84.12**	**83.33**	**78.2**	**45.34**
Synthetic Rainy Dataset	2k	81.42	78.73	72.87	56.37	83.56	**80.46**	74.96	39.18
	4k	**81.55**	**78.84**	**72.94**	56.43	83.45	80.22	75.02	38.65
	8k	81.54	78.79	72.88	**56.71**	**83.66**	80.42	**77.25**	**39.58**
Synthetic Rainy Dataset†	2k	81.33	78.59	72.75	56.9	83.3	80.13	74.09	37.67
	4k	81.24	78.53	72.73	56.69	83.31	79.94	74.39	36.08
	8k	81.37	78.65	74.89	56.72	83.31	80.07	74.60	37.54

TABLE II: Results of 3D object detection with additional data augmentation using Pointpillars [34]. The training data of each experiment comprises the base training set (15k frames under clear weather) along with an additional rainy weather training set. We use average precision(AP) over 40 recall positions where the Intersection over Union(IoU) threshold is set to 0.5 and 0.7, in both bird's eye view(BEV) 2D bounding box IoU and 3D bounding box IoU,
† *the intensity of point cloud is set to a constant value, i.e., eliminating intensity information*

B. Experimental Setup

To validate the realism of 4D synthetic point cloud data generated by our method and the effectiveness of data augmentation in downstream tasks, we reorganize the data from Waymo dataset [25] and the synthetic rainy dataset. We augment the clear weather dataset with the additional rainy dataset to train the perception model and evaluate its performance under real-world weather conditions. Based on weather annotations, we partition the train set of Waymo dataset [25], utilizing 15k frames of clear weather data as the base training set, 4k frames of data in rainy scenes as an additional Waymo Rainy Dataset, along with 2k frames each for the clear weather and rainy weather test sets. The synthetic rainy dataset is also regarded as an additional data source. We define various data blending strategies including cross data source mixing and varying sample quantities.

All experiments are trained from scratch and implemented with MMDetection3D [35]. We selected PointPillars [36], a popular method for 3D object detection as the model for training on the dataset. We use Adam optimizer with a multi-step scheduler, setting the initial learning rate to 0.001 and the weight decay to 0.01. The entire training process concludes upon reaching 24 epochs.

C. Experimental Results

We examine the realism of our synthetic dataset by evaluating the model's performance trained with additional datasets, and results are listed in Table II. Our baseline model is trained by only utilizing the base training set. With the additional Synthetic Rainy Dataset, we can observe that the model has a clear advantage over the baseline. It generally outperforms on Rainy Weather Test Set by around 3% and also maintains accuracy on the Clear Weather Test Set. When employing the Waymo Rainy Dataset as an additional data source, the performance can be continuously increased using real rainy weather data at different scales. Similarly, this phenomenon is also observed with the Synthetic Rainy Dataset, indicating that simulated data positively enhances the model's performance in rainy weather detection. Compared to the difficulty in collecting real data, synthetic data offers a more accessible means to scale up data volume and enhance model performance. The model trained on 8k synthetic rainy data demonstrates performance improvements of 2.17% and 1.57% in terms of AP_{BEV} and AP_{3D} at an IoU threshold of 0.7 when compared to the model trained on 2k real rainy data. This suggests the potential effectiveness of the synthetic dataset. To verify the effectiveness of the intensity, we compare the model results when the point cloud intensity is unavailable. It shows that the model with intensity information performs better under different synthetic data samples. The experimental results indicate that our synthetic point cloud data, generated through simulator-based emulation and point cloud intensity network prediction, closely approximates the characteristics of the Waymo dataset [25], thereby supporting the realism of our synthetic data.

VI. Conclusions

In this work, our primary goal is to achieve realistic simulation for LiDARs under rainy weather conditions. We introduce a simulator-based physical modeling approach for realistic rain simulation, specifically focusing on the spray phenomenon, and develop a weather-based intensity prediction network to complement the point cloud intensity. We propose a data generation pipeline for creating synthetic datasets with the reconstruction of the traffic scenarios in the simulator. The experimental results show the synthetic data we generated effectively bridges the domain gap, enhancing the model's robustness in rainy weather conditions.

Acknowledgement. This research is supported in part by National Science and Technology Major Project (2022ZD0115502), National Natural Science Foundation of China (NO. 62122010, U23B2010), Zhejiang Provincial Natural Science Foundation of China (Grant No. LDT23F02022F02), Beijing Natural Science Foundation (NO. L231011) and Beihang World TOP University Cooperation Program. The research is also supported by Shanghai Artificial Intelligence Laboratory, the National Key R&D Program of China (Grant No. 2022ZD0160104) and the Science and Technology Commission of Shanghai Municipality (Grant No. 22DZ1100102).

REFERENCES

[1] Y. Li, P. Duthon, M. Colomb, and J. Ibanez-Guzman, "What happens for a tof lidar in fog?" *IEEE Transactions on Intelligent Transportation Systems*, vol. 22, no. 11, pp. 6670–6681, 2020.

[2] S. Li, Z. Wang, F. Juefei-Xu, Q. Guo, X. Li, and L. Ma, "Common corruption robustness of point cloud detectors: Benchmark and enhancement," *arXiv preprint arXiv:2210.05896*, 2022.

[3] Y. Dong, C. Kang, J. Zhang, Z. Zhu, Y. Wang, X. Yang, H. Su, X. Wei, and J. Zhu, "Benchmarking robustness of 3d object detection to common corruptions," in *Proceedings of the IEEE/CVF Conference on Computer Vision and Pattern Recognition*, 2023, pp. 1022–1032.

[4] M. Hahner, D. Dai, A. Liniger, and L. Van Gool, "Quantifying data augmentation for lidar based 3d object detection," *arXiv preprint arXiv:2004.01643*, 2020.

[5] M. Dreissig, D. Scheuble, F. Piewak, and J. Boedecker, "Survey on lidar perception in adverse weather conditions," *arXiv preprint arXiv:2304.06312*, 2023.

[6] C. Sakaridis, D. Dai, and L. Van Gool, "Semantic foggy scene understanding with synthetic data," *International Journal of Computer Vision*, vol. 126, pp. 973–992, 2018.

[7] M. Tremblay, S. S. Halder, R. De Charette, and J.-F. Lalonde, "Rain rendering for evaluating and improving robustness to bad weather," *International Journal of Computer Vision*, vol. 129, pp. 341–360, 2021.

[8] M. J. Mirza, M. Masana, H. Possegger, and H. Bischof, "An efficient domain-incremental learning approach to drive in all weather conditions," in *Proceedings of the IEEE/CVF Conference on Computer Vision and Pattern Recognition (CVPR) Workshops*, June 2022, pp. 3001–3011.

[9] R. Heinzler, P. Schindler, J. Seekircher, W. Ritter, and W. Stork, "Weather influence and classification with automotive lidar sensors," in *2019 IEEE intelligent vehicles symposium (IV)*. IEEE, 2019, pp. 1527–1534.

[10] C. Goodin, D. Carruth, M. Doude, and C. Hudson, "Predicting the influence of rain on lidar in adas," *Electronics*, vol. 8, no. 1, p. 89, 2019.

[11] V. Kilic, D. Hegde, V. Sindagi, A. B. Cooper, M. A. Foster, and V. M. Patel, "Lidar light scattering augmentation (lisa): Physics-based simulation of adverse weather conditions for 3d object detection," *arXiv preprint arXiv:2107.07004*, 2021.

[12] M. Hahner, C. Sakaridis, D. Dai, and L. Van Gool, "Fog simulation on real lidar point clouds for 3d object detection in adverse weather," in *Proceedings of the IEEE/CVF International Conference on Computer Vision*, 2021, pp. 15 283–15 292.

[13] Y. Liu, Y. Tian, B. Sun, Y. Wang, and F.-Y. Wang, "Parallel lidars meet the foggy weather," *IEEE Journal of Radio Frequency Identification*, vol. 6, pp. 867–870, 2022.

[14] M. Hahner, C. Sakaridis, M. Bijelic, F. Heide, F. Yu, D. Dai, and L. Van Gool, "Lidar snowfall simulation for robust 3d object detection," in *Proceedings of the IEEE/CVF Conference on Computer Vision and Pattern Recognition*, 2022, pp. 16 364–16 374.

[15] A. Dosovitskiy, G. Ros, F. Codevilla, A. Lopez, and V. Koltun, "Carla: An open urban driving simulator," in *Conference on robot learning*. PMLR, 2017, pp. 1–16.

[16] T. Yang, Y. Li, Y. Ruichek, and Z. Yan, "Lanoising: A data-driven approach for 903nm tof lidar performance modeling under fog," in *2020 IEEE/RSJ International Conference on Intelligent Robots and Systems (IROS)*. IEEE, 2020, pp. 10 084–10 091.

[17] C. F. Bohren and D. R. Huffman, *Absorption and scattering of light by small particles*. John Wiley & Sons, 2008.

[18] J. R. V. Rivero, T. Gerbich, B. Buschardt, and J. Chen, "The effect of spray water on an automotive lidar sensor: A real-time simulation study," *IEEE Transactions on Intelligent Vehicles*, vol. 7, no. 1, pp. 57–72, 2021.

[19] D. H. Weir, J. F. Strange, R. K. Heffley, *et al.*, "Reduction of adverse aerodynamic effects of large trucks, volume i. technical report," United States. Federal Highway Administration, Tech. Rep., 1978.

[20] Y.-C. Shih, W.-H. Liao, W.-C. Lin, S.-K. Wong, and C.-C. Wang, "Reconstruction and synthesis of lidar point clouds of spray," *IEEE Robotics and Automation Letters*, vol. 7, no. 2, pp. 3765–3772, 2022.

[21] C. Linnhoff, D. Scheuble, M. Bijelic, L. Elster, P. Rosenberger, W. Ritter, D. Dai, and H. Winner, "Simulating road spray effects in automotive lidar sensor models," *arXiv preprint arXiv:2212.08558*, 2022.

[22] B. Wu, X. Zhou, S. Zhao, X. Yue, and K. Keutzer, "Squeezesegv2: Improved model structure and unsupervised domain adaptation for road-object segmentation from a lidar point cloud," in *2019 international conference on robotics and automation (ICRA)*. IEEE, 2019, pp. 4376–4382.

[23] S. Manivasagam, S. Wang, K. Wong, W. Zeng, M. Sazanovich, S. Tan, B. Yang, W.-C. Ma, and R. Urtasun, "Lidarsim: Realistic lidar simulation by leveraging the real world," in *Proceedings of the IEEE/CVF Conference on Computer Vision and Pattern Recognition*, 2020, pp. 11 167–11 176.

[24] P. Vacek, O. Jašek, K. Zimmermann, and T. Svoboda, "Learning to predict lidar intensities," *IEEE Transactions on Intelligent Transportation Systems*, vol. 23, no. 4, pp. 3556–3564, 2021.

[25] P. Sun, H. Kretzschmar, X. Dotiwalla, A. Chouard, V. Patnaik, P. Tsui, J. Guo, Y. Zhou, Y. Chai, B. Caine, *et al.*, "Scalability in perception for autonomous driving: Waymo open dataset," in *Proceedings of the IEEE/CVF conference on computer vision and pattern recognition*, 2020, pp. 2446–2454.

[26] S. Hasirlioglu and A. Riener, "Introduction to rain and fog attenuation on automotive surround sensors," in *2017 IEEE 20th International Conference on Intelligent Transportation Systems (ITSC)*. IEEE, 2017, pp. 1–7.

[27] A. P. Gaylard, K. Kirwan, and D. A. Lockerby, "Surface contamination of cars: A review," *Proceedings of the Institution of Mechanical Engineers, Part D: Journal of Automobile Engineering*, vol. 231, no. 9, pp. 1160–1176, 2017.

[28] A. P. Gaylard and B. Duncan, "Simulation of rear glass and body side vehicle soiling by road sprays," *SAE International Journal of Passenger Cars-Mechanical Systems*, vol. 4, no. 2011-01-0173, pp. 184–196, 2011.

[29] T. Hagemeier, M. Hartmann, and D. Thévenin, "Practice of vehicle soiling investigations: A review," *International Journal of Multiphase Flow*, vol. 37, no. 8, pp. 860–875, 2011.

[30] G. Yan, C. Xia, H. Zhou, H. Zhu, and Z. Yang, "Experimental investigation of the bi-stable behavior in the wake of a notchback mira model," SAE Technical Paper, Tech. Rep., 2019.

[31] O. Ronneberger, P. Fischer, and T. Brox, "U-net: Convolutional networks for biomedical image segmentation," in *Medical Image Computing and Computer-Assisted Intervention–MICCAI 2015: 18th International Conference, Munich, Germany, October 5-9, 2015, Proceedings, Part III 18*. Springer, 2015, pp. 234–241.

[32] X. Cai, W. Jiang, R. Xu, W. Zhao, J. Ma, S. Liu, and Y. Li, "Analyzing infrastructure lidar placement with realistic lidar simulation library," in *2023 IEEE International Conference on Robotics and Automation (ICRA)*, 2023, pp. 5581–5587.

[33] R. Xu, Y. Guo, X. Han, X. Xia, H. Xiang, and J. Ma, "Opencda: an open cooperative driving automation framework integrated with co-simulation," in *2021 IEEE International Intelligent Transportation Systems Conference (ITSC)*. IEEE, 2021, pp. 1155–1162.

[34] A. H. Lang, S. Vora, H. Caesar, L. Zhou, J. Yang, and O. Beijbom, "Pointpillars: Fast encoders for object detection from point clouds," in *Proceedings of the IEEE/CVF Conference on Computer Vision and Pattern Recognition (CVPR)*, June 2019.

[35] M. Contributors, "MMDetection3D: OpenMMLab next-generation platform for general 3D object detection," https://github.com/open-mmlab/mmdetection3d, 2020.

[36] A. H. Lang, S. Vora, H. Caesar, L. Zhou, J. Yang, and O. Beijbom, "Pointpillars: Fast encoders for object detection from point clouds," in *Proceedings of the IEEE/CVF conference on computer vision and pattern recognition*, 2019, pp. 12 697–12 705.